

A variational multiscale method derived from an adaptive stabilized conforming finite element method via residual minimization on dual norms

Juan F. Giraldo^{a,b,*}, Victor M. Calo^a

^a*School of Electrical Engineering, Computing & Mathematical Sciences, Curtin University, Australia*

^b*Mineral Resources, Commonwealth Scientific and Industrial Research Organisation (CSIRO), Australia*

Abstract

This paper interprets the stabilized finite element method via residual minimization as a variational multiscale method. We approximate the solution to the partial differential equations using two discrete spaces that we build on a triangulation of the domain; we denote these spaces as coarse and enriched spaces. Building on the adaptive stabilized finite element method via residual minimization, we find a coarse-scale approximation in a continuous space by minimizing the residual on a dual discontinuous Galerkin norm; this process allows us to compute a robust error estimate to construct an on-the-fly adaptive method. We reinterpret the residual projection using the variational multiscale framework to derive a fine-scale approximation. As a result, on each mesh of the adaptive process, we obtain stable coarse- and fine-scale solutions derived from a symmetric saddle-point formulation and an a-posteriori error indicator to guide automatic adaptivity. We test our framework in several challenging scenarios for linear and nonlinear convection-dominated diffusion problems to demonstrate the framework's performance in providing stability in the solution with optimal convergence rates in the asymptotic regime and robust performance in the pre-asymptotic regime. Lastly, we introduce a heuristic dual-term contribution in the variational form to improve the full-scale approximation for symmetric formulations (e.g., diffusion problem).

Keywords: Multiscale problems, Variational multiscale method (VMS), Residual Minimization, Convection-dominated diffusion equation, Stabilized finite elements, Adaptive mesh refinement, Automatic spatial adaptivity

1. Introduction

The convection-dominated diffusion equation is a challenging model problem for several physics and engineering applications due to its singularly perturbed behaviour for high Péclet numbers, leading to singularities such as sharp inner and boundary layers. Brooks and Hughes [1] introduced the streamline-upwind Petrov-Galerkin (SUPG) method to overcome some of these difficulties. This method adds a residual-based stabilizing term to induce a numerical diffusion along the streamlines, which enhances control and stability in the convective operator while conserving consistency in the formulation. The Galerkin/least-squares method (GLS) [2] generalizes this idea by adding a least-squares term to the stabilization to enhance control of the whole residual. Although these methods have proven effective at stabilizing the numerical solution of convection-dominated problems, the accuracy of these approaches highly depends on a user-defined stabilization parameter, which requires tuning in most real-world challenges [3]. In 1998, Hughes [4] unified these ideas introducing the variational multiscale method (VMS). This method captures the variational subscales and improves stability properties while maintaining the consistency of the former residual-based methods [5–16]. VMS decomposes the solution into two scales and keeps their coupling to approximate the fine-scale

*Corresponding author

Email address: jfgiraldo@gmail.com (Juan F. Giraldo)

solution effect that a given mesh cannot capture [17–20]. The VMS paradigm led to a reinterpretation of the traditional residual-based methods as approximate sub-grid scale models and identified the unresolved fine scales as an essential key in the stabilization, even for linear systems including the advection-diffusion equations [21–23]. Related scale-separation models were generalized and extended to diverse applications such as turbulence modeling and wave propagation [24–29]. Cohen et al. [30] extended the stabilization ideas with least-squares/minimum residual minimization in GLS for more general dual norms. They introduced a saddle point formulation of this residual method, which refers to a VMS formulation. These ideas are extended in the Discontinuous Petrov-Galerkin method (DPG) [31–37] using different non-standard dual norms for stabilization [38–44]. DPG is introduced in the context of a VMS for the convection-diffusion equation in [45], offering an alternative, well-behaved sub-grid model to approximate the fine scale [40, 43, 46]. The Discontinuous Galerkin Method (dG), initially proposed in 1973 by Reed and Hill [47], has offered an alternative stabilization technique over the last few decades and was rapidly extended in numerous applications due to its good stability properties [48–52]. dG is advantageous over classical methods in providing robustness and high-order accurate approximations, especially for advective operators associated with hyperbolic equations [53]. Its stability is induced by the numerical fluxes imposed on internal element interfaces, leading to discretely stable solutions with local conservation. dG is related to residual-based stabilization methods in [52–54] and is used for new stabilized methods based on VMS, including the Multiscale Discontinuous Galerkin method (MSDG) [55–57], the Discontinuous residual-free bubble method [58], among other recent approaches [59, 60]. Alternative stabilization techniques that generalize dG ideas are the Interior Penalty methods that use continuous functions and can handle difficulties encountered by continuous finite element methods in advection-diffusion problems [61, 62]. These methods penalize flux jumps at mesh interfaces and were applied to biharmonic operators and second-order elliptic and parabolic problems [62]. Burman and collaborators have advanced the error estimates for interior penalty methods [63, 64] and generalized the ideas to introduce the high-order Continuous Interior Penalty (CIP) finite element method [65, 66]. Effectively, Burman [67] introduced a formulation relating stabilized continuous and discontinuous Galerkin frameworks with the CIP formulation. Calo et al. [68] introduced a conforming finite element method that constructs a discrete approximation by minimizing the residual on a dual discontinuous Galerkin norm. This method combines the residual minimization ideas used in DPG with the reliability and inf-sup stability offered by dG. This framework builds on a long tradition of adaptive finite element techniques [46, 69–72] and were applied to several steady and unsteady partial differential equations [68, 73–80]. We recently used CIP as the coercive discretization for continuous spaces as the underlying stable method to build an adaptive stabilized finite element method via residual minimization that uses continuous solutions that require much fewer degrees of freedom than dG on a given mesh [81, 82]. This paper presents a new method integrating ideas from [68] to derive a residual minimization approach from a VMS perspective. Our method builds on the concepts from MSDG to decompose a full-discrete discontinuous finite element space into discontinuous (fine) and continuous (coarse) components and leverages VMS analysis to define an inter-scale operator. We begin with an arbitrary discontinuous finite element space and derive a continuous representation by minimizing the residual on a dual discontinuous Galerkin norm. Using the VMS analysis and the residual representative obtained from the dual Galerkin orthogonality, we derive an inter-scale problem to define the stable fine-scale contribution and an error estimator to guide adaptivity. Our approach results in a stable coarse- and fine-scale solution derived from a symmetric saddle-point formulation and an a-posteriori error indicator. We validate our method by tackling challenging linear advection-dominated problems and extend our approach for scalar nonlinear conservation laws by using the Lax-Friedrichs flux within the dG context [51, 83, 84]. The aims of this paper are: first, to introduce the residual minimization method in [68] as a variational multiscale method; secondly, to demonstrate the performance of the fine-scale approximation and its influence on the full-scale approximation in terms of stability and convergence for challenging steady linear and nonlinear convection-dominated diffusion equations. The remainder of the paper is organized as follows: Section 2 introduces the continuous problems and the discontinuous discretization. Section 3 describes the residual minimization strategy. Section 4 presents the variational multiscale formulation. Section 5 shows numerical examples of linear problems. Section 6 extends this approach to nonlinear systems of conservation laws. Finally, we conclude the document with some closing remarks.

2. Continuous problem and discontinuous discretization

2.1. Advection-diffusion equation

Let $\Omega \subset \mathbb{R}^d$ with $d = 2, 3$ being a bounded domain with boundary $\Gamma := \partial\Omega$. Let $\kappa \in [L^\infty(\Omega)]^{d,d}$ represent a positive definite diffusion tensor and $\beta \in [L^\infty(\Omega)]^d$ a smooth velocity field. Let \mathbf{n} be the outward unit normal vector with respect to Γ ; we define the inflow and outflow boundaries, respectively, by

$$\Gamma^- := \{x \in \Gamma \mid \beta \cdot \mathbf{n} < 0\}, \quad \Gamma^+ := \{x \in \Gamma \mid \beta \cdot \mathbf{n} \geq 0\}.$$

We denote by Γ_D the Dirichlet and Γ_N the Neumann boundary functions, which are a complementary subset of Γ (i.e., $\Gamma = \Gamma_N \cup \Gamma_D$). Thus, we define the inner and outer parts of the Neumann boundary as follow:

$$\Gamma_N^- := \Gamma_N \cap \Gamma^-, \quad \Gamma_N^+ := \Gamma_N \cap \Gamma^+. \quad (1)$$

We consider the following advection-diffusion equation in strong form as:

$$\begin{aligned} -\operatorname{div}(\kappa \nabla u) + \beta \cdot \nabla u &= f && \text{in } \Omega, \\ u &= u_D && \text{on } \Gamma_D, \\ (-\beta u + \kappa \nabla u) \cdot \mathbf{n} &= h_N && \text{on } \Gamma_N^-, \\ \kappa \nabla u \cdot \mathbf{n} &= h_N && \text{on } \Gamma_N^+, \end{aligned} \quad (2)$$

where we denote $f \in L_2(\Omega)$ as the source term and $u_D \in H^{-1/2}(\Gamma_D)$ and $h_N \in H^{-1/2}(\Gamma_N)$ as the Dirichlet and Neumann boundary functions, respectively. Following the function spaces $V := \{v \in H^1(\Omega) : v|_{\Gamma_D} = 0\}$ and $\tilde{V} := \{u \in H^1(\Omega) : u|_{\Gamma_D} = u_D\}$, the continuous weak variational formulation of (2) reads:

$$\begin{cases} \text{Find } u \in \tilde{V} \text{ such that:} \\ (\nabla v, \kappa \nabla u)_\Omega + (v, \beta \cdot \nabla u)_\Omega + (v, (\beta \cdot \mathbf{n})u)_{\Gamma^-} = (v, f)_\Omega + (v, h_N)_{\Gamma_N}, \quad \forall v \in V, \end{cases} \quad (3)$$

where $(\cdot, \cdot)_\Omega$ and $(\cdot, \cdot)_\Gamma$ denote the L_2 -scalar product on Ω and Γ , respectively.

2.2. Discontinuous Galerkin (dG) discretization

Let \mathfrak{T} be a coarse triangulation, such that Ω is decomposed into n subdomains K as $\mathfrak{T} : \{K_i\}_{i=1}^n$. We define the broken space of discontinuous functions as:

$$\mathbb{V}_h := \{v \in L_2(\mathfrak{T}) : v|_K \in \mathbb{P}^p(K) \in, \forall K \in \mathfrak{T}\}, \quad (4)$$

where \mathbb{P}^p denotes the set of functions of degree lower than or equal to p . Let K_1 and K_2 represent two disjoint elements in \mathfrak{T} , and let F be their shared face. We define the set of all faces as $\mathcal{S}_h := \bigcup_{K \in \mathfrak{T}} F$. We further define the set of interior faces by $\mathcal{S}_h^0 = \mathcal{S}_h \setminus \Gamma$ and the set of boundary faces by $\mathcal{S}_h^\partial = \mathcal{S}_h \cap \Gamma$. We also define the set of inflow boundary faces as $\mathcal{S}_h^{\partial^-} := \mathcal{S}_h^\partial \cap \Gamma^-$, the set of outflow boundary faces as $\mathcal{S}_h^{\partial^+} := \mathcal{S}_h^\partial \cap \Gamma^+$, and we denote by $\mathcal{S}_h^D = \mathcal{S}_h \cap \Gamma^D$ and $\mathcal{S}_h^N = \mathcal{S}_h \cap \Gamma^N$ the sets of Dirichlet and Neumann faces, respectively. Let h_K be the element diameter, h_F the face diameter, and \mathbf{n}_F be the unit normal vector in the outer direction of F from K_1 to K_2 . Given a scalar field v and denoting $v_{1,2} := v|_{K_1, K_2}$, we define the arithmetic average $\{v\}$, weighted average $\{v\}_\omega$ and jump $[[v]]$ on an internal face $F \in \mathcal{S}_h^0$ by

$$\{v\} := \frac{1}{2}(v_1 + v_2), \quad \{v\}_\omega := v_1 \omega_1 + v_2 \omega_2, \quad [[v]] := v_1 - v_2,$$

where $\omega_1 + \omega_2 = 1$ and $\omega_1, \omega_2 \geq 0$. For heterogeneous diffusion, we use:

$$\omega_1 = \frac{\delta_1}{\delta_1 + \delta_2}, \quad \omega_2 = \frac{\delta_2}{\delta_1 + \delta_2}, \quad (5)$$

with $\delta_1 = \mathbf{n}_F \cdot \kappa_1 \mathbf{n}_F$ and $\delta_2 = \mathbf{n}_F \cdot \kappa_2 \mathbf{n}_F$. In the homogeneous diffusion case, these weights reduce to $\omega_1 = \omega_2 = \frac{1}{2}$, recovering the arithmetic average. We set on boundary faces $F \in \mathcal{S}_h^\partial$ that $\{v\} = \{v\}_\omega = \llbracket v \rrbracket = v$. For further details in the discrete setting, see [85]. We use the following dG discrete form:

$$\begin{cases} \text{Find } u_h \in \mathbb{V}_h, \text{ such that:} \\ b_h(v_h, u_h) = \ell_h(v_h) \quad \forall v_h \in \mathbb{V}_h, \end{cases} \quad (6)$$

where b_h defines the dG discrete bilinear form considering the contribution of the diffusive part from the Symmetric Weighted Interior Penalty form (SWIP) and the advective part from the upwinding formulation:

$$b_h(v, u) := b_h(v, u)^{\text{swip}} + b_h(v, u)^{\text{upw}}, \quad (7)$$

with,

$$\begin{aligned} b_h(v, u)^{\text{swip}} &:= \sum_{K \in \mathfrak{T}} (\nabla_h v, \kappa \nabla_h u)_K \\ &\quad - \sum_{F \in \mathcal{S}_h^0} \left((\llbracket v \rrbracket, \{\kappa \nabla_h u\}_\omega \cdot \mathbf{n}_F)_F + (\{\kappa \nabla_h v\}_\omega \cdot \mathbf{n}_F, \llbracket u \rrbracket)_F - \eta_e \gamma_\kappa (\llbracket v \rrbracket, \llbracket u \rrbracket)_F \right) \\ &\quad - \sum_{F \in \mathcal{S}_h^D} \left((v, \kappa \nabla_h u \cdot \mathbf{n}_F)_F + (\kappa \nabla_h v \cdot \mathbf{n}_F, u)_F - \eta_e \gamma_\kappa (v, u)_F \right), \end{aligned} \quad (8)$$

$$\begin{aligned} b_h(v, u)^{\text{upw}} &:= \sum_{K \in \mathfrak{T}} (v, \beta \cdot \nabla u)_K + \sum_{F \in \mathcal{S}_h^{\partial^-}} (v, (\beta \cdot \mathbf{n}_F) u)_F \\ &\quad + \sum_{F \in \mathcal{S}_h^0} \left((\llbracket v \rrbracket, \frac{1}{2} |\beta \cdot \mathbf{n}_F| \llbracket u \rrbracket)_F - (\{v\}, (\beta \cdot \mathbf{n}_F) \llbracket u \rrbracket)_F \right), \end{aligned} \quad (9)$$

where $(\cdot, \cdot)_F$ and $(\cdot, \cdot)_K$ represent the inner product over the discrete face and internal element, respectively. The diffusion penalty γ_κ is defined for all internal faces $F \in \mathcal{S}_h^0$ as:

$$\gamma_\kappa := \frac{2\kappa_1 \kappa_2}{\kappa_1 + \kappa_2},$$

and η_e denotes a positive penalty defined as [86]:

$$\eta_e := \frac{(p+1)(p+d)}{d} \begin{cases} \frac{1}{2} \left(\frac{\mathcal{A}(\partial K_1)}{\mathcal{V}(K_1)} + \frac{\mathcal{A}(\partial K_2)}{\mathcal{V}(K_2)} \right), & \text{if } F = \partial K_1 \cap \partial K_2, \\ \frac{\mathcal{A}(\partial K)}{\mathcal{V}(K)}, & \text{if } F = \partial K \cap \Gamma, \end{cases} \quad (10)$$

where d denotes the problem dimension, and p represents the polynomial degree of the test space. In 3D, \mathcal{V} and \mathcal{A} denote the volume and area of an element, respectively. In 2D, they represent the length and area of the element. The right-hand side in (6) reads for weakly imposed non-homogeneous Dirichlet and Neumann boundary conditions as:

$$\begin{aligned} \ell_h(v) &:= \sum_{K \in \mathfrak{T}} (v, f) + \sum_{F \in \mathcal{S}_h^D} (\eta_e \kappa (v, u_D)_F - (\kappa \nabla_h v \cdot \mathbf{n}_F, u_D)_F) \\ &\quad - \sum_{F \in \mathcal{S}_h^D \cap \Gamma^-} (v, (\beta \cdot \mathbf{n}_F) u_D)_F + \sum_{F \in \mathcal{S}_h^N} (v, h_N)_F. \end{aligned} \quad (11)$$

We endow \mathbb{V}_h with the norm:

$$\|w\|_{\mathbb{V}_h}^2 := \|w\|_{\text{upw}}^2 + \|w\|_{\text{swip}}^2, \quad (12)$$

with

$$\|w\|_{\text{adv}}^2 := \|w\|_0^2 + \sum_{F \in \mathcal{F}_h} \left(\frac{1}{2} |\beta \cdot \mathbf{n}_F| \llbracket w \rrbracket, \llbracket w \rrbracket \right)_{0,F} + \sum_{K \in \mathcal{T}} h_K \|\beta \cdot \nabla w\|_{0,K}^2, \quad (13)$$

$$\|w\|_{\text{swip}}^2 := \|\kappa \nabla w\|_0^2 + \sum_{F \in \mathcal{F}_h} (\eta_e \kappa \llbracket w \rrbracket, \llbracket w \rrbracket)_{0,F}, \quad (14)$$

where $\|\cdot\|_0$ represents the L_2 -norm on the domain Ω and $\|\cdot\|_{0,\Gamma}$ on its boundary Γ , while $\|\cdot\|_{0,K}$ and $\|\cdot\|_{0,F}$ denote the L_2 -norm on the element K and faces F , respectively. Problem (6) is well-posed, and the inf-sup stability is established through the norm (12). Refer to [49] for further details. The sub-index h for the test and trial solutions (i.e., u_h and v_h) are dropped in the following sections to keep the notation simple.

3. Residual minimization formulation

This section briefly recaps the residual minimization strategy described in [68]. The main idea is to deliver a stable approximation in a continuous space by minimizing the residual onto a discontinuous Galerkin norm. First, we define a subspace $\bar{\mathbb{V}}_h \subset \mathbb{V}_h$, such that $\bar{\mathbb{V}}_h$ is the H^1 -conforming subspace. Then, from the stable formulation in (6), we use the trial subspace $\bar{\mathbb{V}}_h$ to solve the following minimization problem:

$$\begin{cases} \text{Find } \bar{u} \in \bar{\mathbb{V}}_h \subset \mathbb{V}_h, \text{ such that:} \\ \bar{u} = \arg \min_{z \in \bar{\mathbb{V}}_h} \frac{1}{2} \|\ell_h - B_h z\|_{\bar{\mathbb{V}}_h^*}^2, \end{cases} \quad (15)$$

where the operator B_h is defined by $\langle \cdot, B_h w \rangle_{\mathbb{V}_h \times \mathbb{V}_h^*} := b_h(\cdot, w), \forall w \in \mathbb{V}_h$. We state (15) as a critical point of the minimizing functional, which can be translated into the following linear problem:

$$\begin{cases} \text{Find } \bar{u} \in \bar{\mathbb{V}}_h, \text{ such that:} \\ (B_h \delta u, \ell_h - B_h \bar{u})_{\mathbb{V}_h^*} = g(R_{\bar{\mathbb{V}}_h}^{-1} B_h \delta u, R_{\bar{\mathbb{V}}_h}^{-1} (\ell_h - B_h \bar{u})) = 0 \quad \forall \delta u \in \bar{\mathbb{V}}_h, \end{cases} \quad (16)$$

where $g(\cdot, \cdot)$ represents the inner product that induces the discrete norm $\|\cdot\|_{\mathbb{V}_h}$ and $R_{\mathbb{V}_h}$ denotes the Riesz operator which maps the elements in \mathbb{V}_h to the dual space \mathbb{V}_h^* , such that:

$$\langle \cdot, R_{\mathbb{V}_h} y \rangle_{\mathbb{V}_h \times \mathbb{V}_h^*} := g(\cdot, y). \quad (17)$$

Defining the residual representation function as

$$\varepsilon := R_{\bar{\mathbb{V}}_h}^{-1} (\ell_h - B_h \bar{u}) \in \mathbb{V}_h,$$

which implies

$$g(\varepsilon, v) = l_h(v) - b_h(u, v), \quad \forall v \in \mathbb{V}_h;$$

thus, the residual minimization problem in (15) leads to the saddle point problem:

$$\begin{cases} \text{Find } (\varepsilon, \bar{u}) \in \mathbb{V}_h \times \bar{\mathbb{V}}_h, \text{ such that:} \\ g(v, \varepsilon) + b_h(v, \bar{u}) + b_h(\varepsilon, \bar{w}) = l_h(v), \quad \forall (v, \bar{w}) \in (\mathbb{V}_h, \bar{\mathbb{V}}_h), \end{cases} \quad (18)$$

where orthogonality condition between the residual representation and the H^1 -conforming subspace of \mathbb{V}_h is enforced as $b_h(\varepsilon, \bar{w}) = 0$. Features of the methodology and the properties of the error estimator and continuous solution are discussed in detail in [68, 74] in the context of advection-reaction-diffusion equations.

4. A variational multiscale interpretation of the residual minimization framework

4.1. A multiscale partition of the trial and test spaces

Following the variational multiscale arguments, we decompose \mathbb{V}_h into coarse and fine scales. Since we use a Petrov-Galerkin formalism, our test and trial spaces are different. Thus, starting from the H^1 -conforming solution space $\bar{\mathbb{V}}_h$ and define appropriate direct sum partitions of the entire function space \mathbb{V}_h using the operators from the residual minimization framework.

First, we define the space \mathbb{V}'_h as the annihilator of the bilinear form $b_h(\cdot, \bar{w}) \forall \bar{w} \in \bar{\mathbb{V}}_h$ (e.g., the residual representative belongs to this set of linear functionals that map the operator's range to zero). Thus, given $\bar{\mathbb{V}}_h \subset \mathbb{V}_h$, we define \mathbb{V}'_h as the annihilator of the bilinear form b_h acting on \mathbb{V}_h , such that

$$\mathbb{V}'_h := \{v \in \mathbb{V}_h \mid b_h(v, \bar{w}) = 0, \quad \forall \bar{w} \in \bar{\mathbb{V}}_h\}, \quad (19)$$

Next, we define $\hat{\mathbb{V}}_h$ as the orthogonal complement of \mathbb{V}'_h with respect to the inner product $g(\cdot, \cdot)$, that is:

$$\hat{\mathbb{V}}_h := \{v \in \mathbb{V}_h \mid g(v, v') = 0, \quad \forall v' \in \mathbb{V}'_h\}. \quad (20)$$

Last, we define the complement of the coarse-scale solution space as the kernel of the bilinear b_h when tested by $\hat{\mathbb{V}}_h$. Thus, given $\hat{\mathbb{V}}_h \subset \mathbb{V}_h$, we define $\tilde{\mathbb{V}}_h$ to be

$$\tilde{\mathbb{V}}_h := \{u \in \mathbb{V}_h \mid b_h(\hat{v}, u) = 0, \quad \forall \hat{v} \in \hat{\mathbb{V}}_h\}. \quad (21)$$

where the (full-scale) trial space is $\mathbb{V}_h := \bar{\mathbb{V}}_h \oplus \tilde{\mathbb{V}}_h$ and the (full-scale) test space is $\mathbb{V}_h := \hat{\mathbb{V}}_h \oplus \mathbb{V}'_h$.

We have a direct sum decomposition of the trial space to deliver a solution $u \in \mathbb{V}_h$ in (6), such that:

$$u = \bar{u} + \tilde{u}. \quad (22)$$

where we denote $\bar{u} \in \bar{\mathbb{V}}_h$ and $\tilde{u} \in \tilde{\mathbb{V}}_h$ as the coarse- and fine-scale trial functions. Similarly, for any test function $v \in \mathbb{V}_h$, we can write

$$v = \hat{v} + v', \quad (23)$$

where we denote $\hat{v} \in \hat{\mathbb{V}}_h$ and $v' \in \mathbb{V}'_h$ as the coarse- and fine-scale test functions. Thus, we have two complementary direct sum decompositions of \mathbb{V}_h .

Thus, the saddle point problem in (18) can be stated as follows:

$$\begin{cases} \text{Find } (\varepsilon', \bar{u}) \in (\mathbb{V}'_h \times \bar{\mathbb{V}}_h), \text{ such that:} \\ g(v, \varepsilon') + b_h(v, \bar{u}) = \ell(v), \quad \forall v \in \mathbb{V}_h \end{cases} \quad (24)$$

Splitting the test function using (23), we reformulate problem (24) as two complementary but independent problems for the coarse-scale solution and the fine-scale residual representative:

- Residual reconstruction (fine-scale problem) as

$$\begin{cases} \text{Find } \varepsilon' \in \mathbb{V}'_h, \text{ such that} \\ g(v', \varepsilon') = \ell(v'), \quad \forall v' \in \mathbb{V}'_h, \end{cases} \quad (25)$$

- H^1 -conforming solution (coarse-scale problem) as

$$\begin{cases} \text{Find } \bar{u} \in \bar{\mathbb{V}}_h, \text{ such that} \\ b_h(\hat{v}, \bar{u}) = \ell(\hat{v}), \quad \forall \hat{v} \in \hat{\mathbb{V}}_h, \end{cases} \quad (26)$$

which corresponds to a Petrov-Galerkin method with optimal test functions [32, 38, 39, 44].

From the definitions of the complementary direct sum decompositions (19)-(21), we have that $b_h(\hat{v}, \tilde{u}) = b_h(v', \tilde{u}) = 0$; thus, problem (6) can be split into the following two problems:

$$\begin{cases} \text{Find } (\bar{u}, \tilde{u}) \in (\bar{\mathbb{V}}_h, \tilde{\mathbb{V}}_h), \text{ such that:} \\ b_h(\hat{v}, u) := b_h(\hat{v}, \bar{u}) = \ell(\hat{v}), & \forall \hat{v} \in \hat{\mathbb{V}}_h, \\ b_h(v', u) := b_h(v', \tilde{u}) = \ell(v'), & \forall v' \in \mathbb{V}'_h. \end{cases} \quad (27)$$

Consequently, from (25) and (27)₂, we can rewrite the fine-scale component of the discrete solution in terms of the residual error estimate

$$b_h(v', \tilde{u}) = g(v', \varepsilon') = \ell(v'), \quad \forall v' \in \mathbb{V}'_h. \quad (28)$$

Thus, we can express (27)₂ such that the fine-scale solution satisfies the following problem:

$$\begin{cases} \text{Find } \tilde{u} \in \tilde{\mathbb{V}}_h, \text{ such that:} \\ b_h(v', \tilde{u}) = g(v', \varepsilon'), \quad \forall v' \in \mathbb{V}'_h. \end{cases} \quad (29)$$

Lastly, since $b(\hat{v}, \tilde{u}) = g(\hat{v}, \varepsilon') = 0$, we can express the fine-scale problem equivalently as

$$\begin{cases} \text{Find } \tilde{u} \in \mathbb{V}_h, \text{ such that:} \\ b_h(v, \tilde{u}) = g(v, \varepsilon'), \quad \forall v \in \mathbb{V}_h. \end{cases} \quad (30)$$

We solve the discrete problem resulting from the system (30) rather than (29) or (27)₂ since the discrete solution is identical, simpler to implement, and cheaper to compute.

Remark 1 (Relation between VMS reconstruction & dG solution). *By construction, the partitioned full-scale approximation in (22) is identical to the classical dG solution. Next, we introduce an adjoint multiscale reconstruction; thus, we denote by (θ) the dG solution of (6).*

4.2. Adjoint multiscale reconstruction

Using the direct sum partitions of the test and trial spaces, we exploit the insight behind the adjoint residual-based estimator proposed for goal-oriented adaptivity in [76]; therein, the authors obtained a residual representative for the quantity of interest by solving a well-posed ad hoc discrete problem. In the present context, this adjoint residual problem is driven by ε' . We introduce the adjoint reconstruction by revisiting the multiscale partitions from the previous section. Given ε' that solves (25), this error representation ε' is proportional to the discrete system's residual [68, 76]. From the definition of \mathbb{V}'_h , we know that

$$b_h(\varepsilon', \bar{v}) = 0, \quad \forall \bar{v} \in \bar{\mathbb{V}}_h.$$

Also, from (30), we have that

$$b_h(v, \tilde{u}) = g(v, \varepsilon'), \quad \forall v \in \mathbb{V}_h;$$

next we add a heuristic interaction of ε' with the whole test space \mathbb{V}_h to the fine-scale driving force. Thus, we postulate the following problem, where the heuristic fine scales $\tilde{u} \in \mathbb{V}'_h$ solve

$$b_h(v, \tilde{u}) = g(v, \varepsilon') + b_h(\varepsilon', v) \quad \forall v \in \mathbb{V}_h. \quad (31)$$

Thus, this heuristic fine-scale postprocessing of the error representative includes two extra contributions:

$$b_h(\hat{v}, \tilde{u}) = b_h(\varepsilon', \hat{v}) \quad \forall \hat{v} \in \hat{\mathbb{V}}_h, \quad (32)$$

$$b_h(v', \tilde{u}) = \ell_h(v') + b_h(\varepsilon', v') \quad \forall v' \in \mathbb{V}'_h, \quad (33)$$

where the first equation contributes to the coarse-scale trial space in $\bar{\mathbb{V}}_h$ while the second one contributes to the fine-scale trial space \mathbb{V}'_h .

In short, we propose the following heuristic adjoint variational multiscale reconstruction such that:

$$\phi = \bar{u} + \tilde{u},$$

where $\tilde{u} \in \mathbb{V}_h$ is the reconstructed fine-scale solution that solves (31) for a given error estimate ε' . In the next section, we test the performance of ϕ in the L_2 and energy (\mathbb{V}_h) norms, showing an improvement in the asymptotic regime, especially for diffusion-dominated problems (i.e., $\|u_{exa} - \phi\|_{\mathbb{V}_h} \lesssim \|u_{exa} - u\|_{\mathbb{V}_h}$).

5. Numerical examples

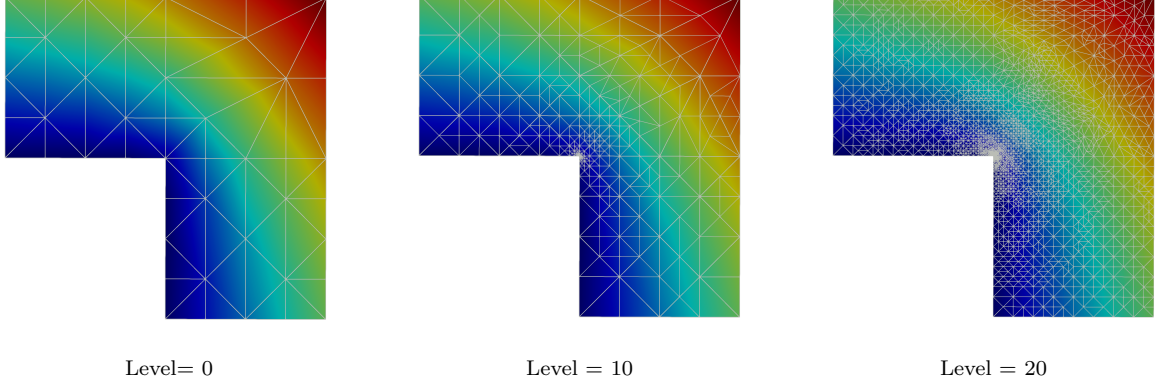


Figure 1: Solution for the re-entrant corner problem for different refinement levels

5.1. Refinement strategy

Next, we demonstrate the efficacy of our methods in different linear cases through a range of numerical examples. We analyze the rate decay for both the coarse and reconstructed full-scale solutions in the L_2 and energy (\mathbb{V}_h) norms and compare these results with the classical dG solution. The convergence plots in the following sections show the error norm versus the total number of degrees of freedom ($DoF^{1/d}$) (i.e., $\dim(\bar{\mathbb{V}}_h) + \dim(\mathbb{V}_h)$). We validate our formulation by evaluating and comparing the performance of our multiscale approach using some test problems described in [74].

We implement an adaptive refinement marking strategy for the following examples using an extended version of the Dörfler bulk-chasing criterion. Our adaptive procedure considers an iterative process in which each iteration consists of the following four steps:

$$\text{SOLVE} \rightarrow \text{ESTIMATE} \rightarrow \text{MARK} \rightarrow \text{REFINE} \quad (34)$$

We mark the elements' contribution to a user-defined fraction (η_{ref}) of the total estimated error $\|\varepsilon\|_{\mathbb{V}_h}^2$. Let η_{ref} be 0.25 and 0.125 for 2D and 3D problems, respectively (see [80] for implementation details). We solve the saddle point problem in (18) employing an iterative algorithm described in [68, 87] and use FEniCS [88] as a platform to perform all the numerical simulations.

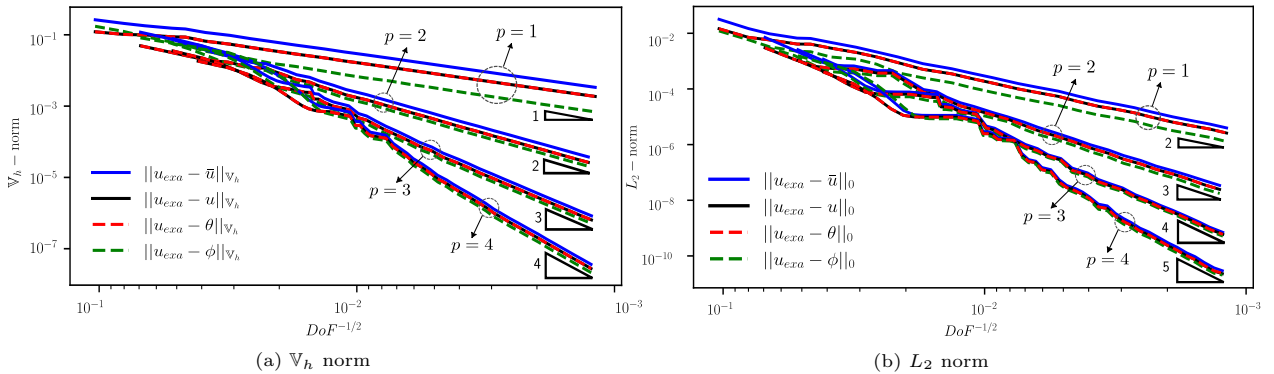


Figure 2: \mathbb{V}_h - & L_2 -norm convergence for Laplace problem

5.2. Diffusion problem for a domain with a re-entrant corner

We study the method's performance with the diffusion problem in a re-entrant corner domain [89]. The problem configuration induces a singularity at the inward-pointing vertex of the concave polygon. Since capturing corner singularities is challenging for uniform refinement techniques, this problem tests the adaptive grid refinement algorithms. We solve the following Laplace equation in an L-shape domain Ω :

$$\begin{aligned} \Delta u &= 0, & \text{in } \Omega &= (-1, 1)^2 \setminus (-1, 0]^2, \\ u &= u_D, & \text{on } \partial\Omega &= \Gamma_D, \end{aligned}$$

where the Dirichlet boundary conditions (u_D) are applied based on the exact solution:

$$u_{exa} = r^\alpha \sin(\alpha\theta),$$

with $r = \sqrt{x^2 + y^2}$, $\theta = \tanh^{-1}(y/x)$ and $\alpha = 2/3$.

Figure 1 shows three surface plots of the full-scale solution and the corresponding meshes for different adaptive refinement levels. The results show the error estimator's robustness and the energy norm's effectiveness at capturing the singularity. Convergence plots are presented in Figure 2 for different test-function polynomial degrees ($p = 1, 2, 3, 4$) in the L_2 and energy norms. Here, we show optimal rate decay for coarse \bar{u} and full-scale \tilde{u} solutions and verify that the fine-scale contribution \tilde{u} recovers the dG approximation θ (i.e., $u \approx \theta$). Besides, Figure 2 shows that the adjoint multiscale reconstruction (ϕ) improves the approximation compared to the full-scale (u) and the dG (θ) solutions regardless of the polynomial degree.

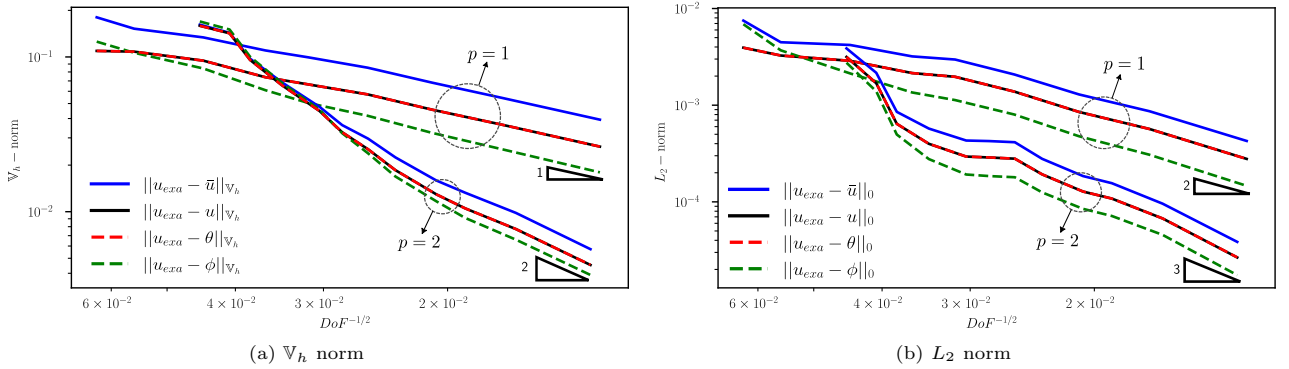


Figure 3: \mathbb{V}_h - and L_2 -norm convergence for Fichera corner, $q = \frac{1}{10}$

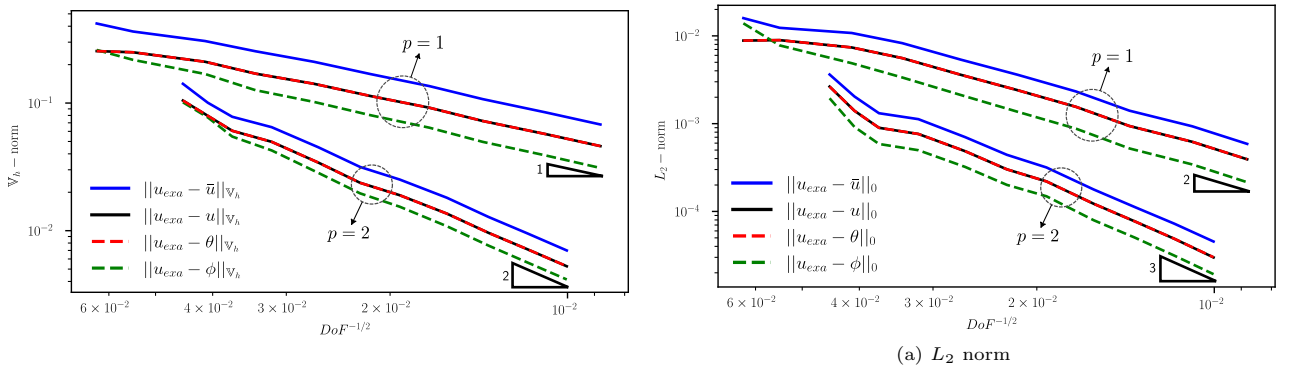


Figure 4: \mathbb{V}_h - and L_2 -norm convergence for Fichera corner, $q = \frac{1}{3}$

5.3. Diffusion problem for a 3D domain with a Fichera corner

In this example, we extend results in Section 5.2 for the 3D Fichera corner problem, where we induce the singularity at the re-entrant corner of the domain $\Omega = (-1, 1)^3 \setminus [0, 1]^3$. We consider the problem:

$$\begin{aligned} -\kappa \Delta u &= f, & \text{in } \Omega, \\ u &= u_D, & \text{on } \Gamma_D, \end{aligned} \quad (35)$$

where $\kappa = 1$ and source term f and Dirichlet boundary conditions (u_D) are derived from the exact solution:

$$u_{\text{exa}} = \left(\sqrt{x^2 + y^2 + z^2} \right)^q$$

with $q = 1/10$ and $q = 1/3$. Similarly to the 2D case, uniform refinement techniques may struggle to accurately capture the behavior in the Fichera corner. The high spatial gradients and the necessity for fine meshes at the singularity lead to suboptimal convergence when no adaptive refinement techniques are used [68]. Figures 3 and 4 display the convergence plots in L_2 and \mathbb{V}_h norms. Here, we test the robustness of the error estimator to provide optimal convergence rates for the coarse solution and to recover the dG solution and optimality in the full-scale solution for different q values. Moreover, as in Section 5.2, the ajoin multiscale reconstruction (ϕ) provides a better approximation compared to the full-scale solution (u) in the L_2 and \mathbb{V}_h norms, and improves the pre-asymptotic convergence rates, especially for linear trial functions.

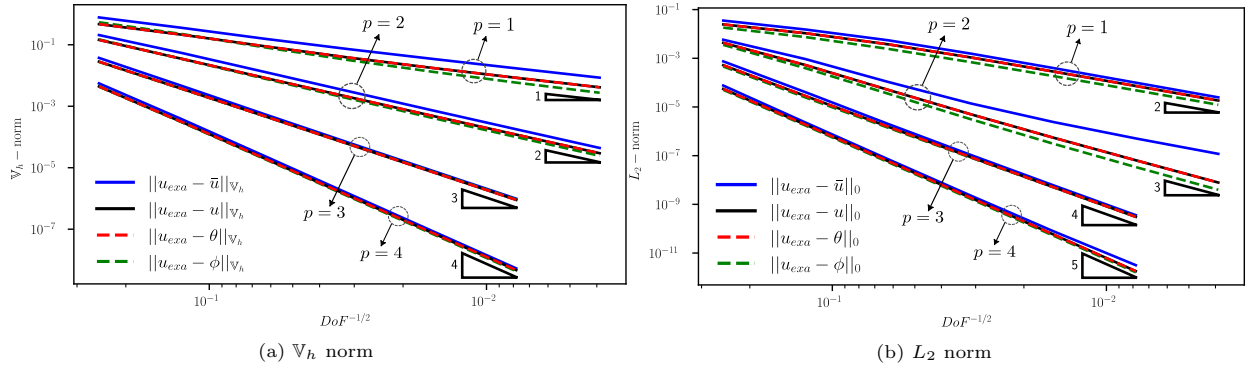


Figure 5: \mathbb{V}_h - & L_2 -norm convergence for heterogeneous diffusion problem

5.4. Heterogeneous Diffusion problem

We solve the advection-diffusion equation with heterogeneous and anisotropic diffusion, following [74]:

$$\begin{aligned} -\kappa \Delta u + \beta \cdot \nabla u &= 0, & \text{in } \Omega, \\ u &= u_D, & \text{on } \Gamma, \end{aligned} \quad (36)$$

where $\beta = (0, 1)^T$ and κ is a second rank tensor with different ϵ_i values for each domain:

$$\kappa|_{\Omega_i} = \begin{pmatrix} \epsilon_i & 0 \\ 0 & 1.0 \end{pmatrix}.$$

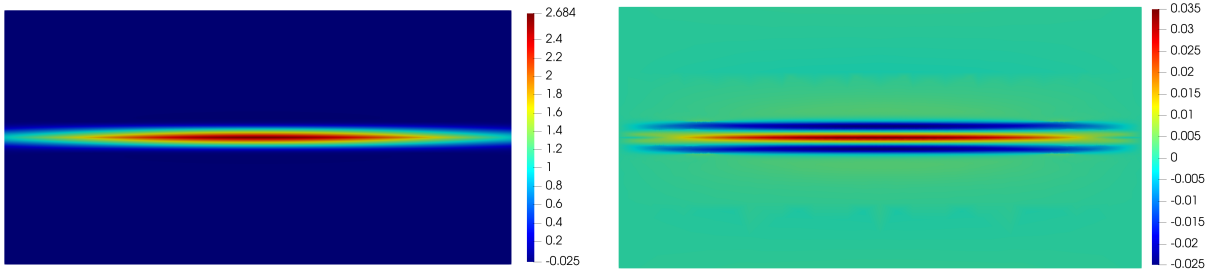
We partition $\Omega = [0, 1]^2$ into two domains: $\Omega_1 = [0, \frac{1}{2}] \times [0, 1]$ and $\Omega_2 = [\frac{1}{2}, 1] \times [0, 1]$, such that $\epsilon_1 = 0.1$ and $\epsilon_2 = 1.0$. We impose Dirichlet boundary conditions (u_D) based on the exact solution for each domain [64]:

$$u_{\text{exa}} = \begin{cases} \left(u_{1/2} - \exp\left(\frac{1}{2\epsilon_1}\right) + (1 - u_{1/2}) \exp\left(\frac{x}{\epsilon_1}\right) \right) / \left(1 - \exp\left(\frac{1}{2\epsilon_1}\right) \right) & \text{if } x \in \Omega_1, \\ \left(-\exp\left(\frac{1}{2\epsilon_2}\right) u_{1/2} + u_{1/2} \exp\left(\frac{x - \frac{1}{2}}{\epsilon_2}\right) \right) / \left(1 - \exp\left(\frac{1}{2\epsilon_2}\right) \right) & \text{if } x \in \Omega_2, \end{cases} \quad (37)$$

where

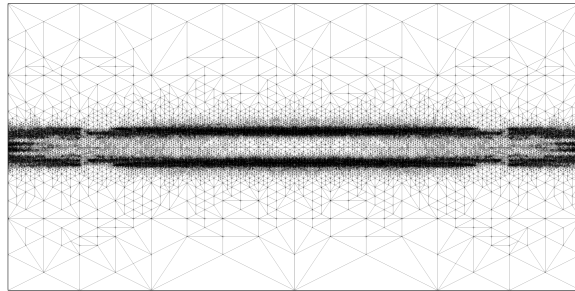
$$u_{1/2} = \left(\frac{\exp\left(\frac{1}{2\epsilon_1}\right)}{1 - \exp\left(\frac{1}{2\epsilon_1}\right)} \right) \left(\frac{\exp\left(\frac{1}{2\epsilon_1}\right)}{1 - \exp\left(\frac{1}{2\epsilon_1}\right)} + \frac{1}{1 - \exp\left(\frac{1}{2\epsilon_2}\right)} \right)^{-1}. \quad (38)$$

Figure 5 plots the convergence in the L_2 and \mathbb{V}_h norms for polynomial orders 1 to 4. As noted in [74], Figure 5(b) shows a loss in the convergence rate in the L_2 norm for the coarse-scale solution (\bar{u}) for even polynomial degrees. However, we can recover dG optimality by including the fine-scale contribution (u'), regardless of the polynomial degree. The adjoint multiscale reconstruction (ϕ) is more accurate than the other discrete approximations on the same mesh.



(a) Coarse-scale solution

(b) Fine-scale solution



(c) Refined mesh

Figure 6: Coarse- & fine-scale solutions with final mesh for strongly anisotropic diffusion problem with $r = 10^6$ & $p = 1$

5.5. Strongly anisotropic diffusion

In this example, we test the performance of our method in a highly anisotropic diffusion problem. We solve equation (35) with high contrast in the permeability tensor:

$$\kappa|_{\Omega} = \begin{pmatrix} \alpha_{\kappa} & 0 \\ 0 & \gamma_{\kappa} \end{pmatrix}. \quad (39)$$

We define the anisotropy ratio, r_{κ} , as the ratio between the maximum and minimum values of the diffusion coefficients; thus, we set $r_{\kappa} := \alpha_{\kappa}/\gamma_{\kappa}$ for (39). High r_{κ} values are challenging in this problem, corresponding to locally small weights in the diffusion tensor, leading to advection-dominated regimes. We study the method's performance by solving (39) for different values of the anisotropy ratio by imposing a sharp inner

layer problem based on the following Gaussian-function-type manufactured solution, as described in [90]:

$$u_{exa} = \frac{\exp(-[x^2 + r_\kappa \tau y^2])}{4\pi\sqrt{r_\kappa\tau}}, \quad (40)$$

with $\tau = 10^{-3}$. We use (40) and $\alpha_\kappa = 1$ to derive the source term (f) and Dirichlet boundary conditions (u_D) in the domain $\Omega = [-1, 1] \times [-0.5, 0.5]$.

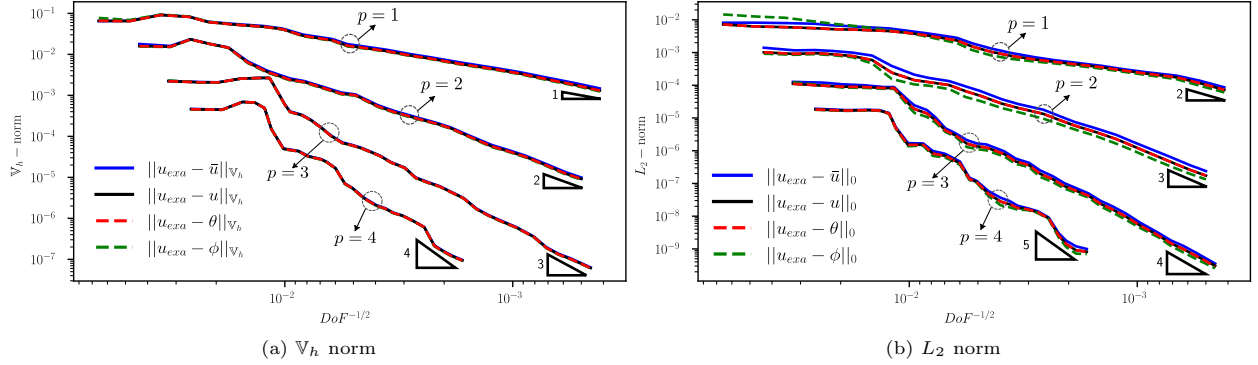


Figure 7: \mathbb{V}_h - and L_2 -norm convergence for anisotropy ratio $r_\kappa = 10^4$.

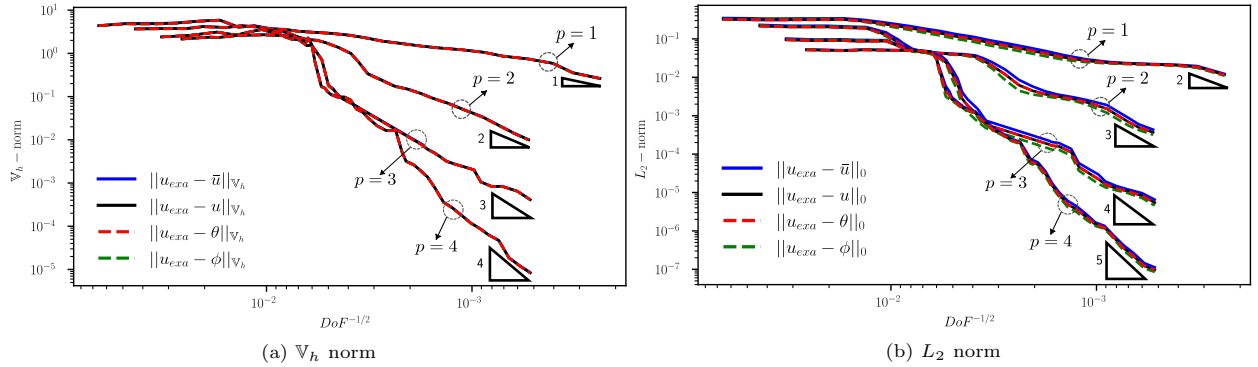


Figure 8: \mathbb{V}_h - and L_2 -norm convergence for anisotropy ratio $r_\kappa = 10^6$.

Figure 6 presents the coarse- and fine-scale solutions showing the discontinuity in $y = 0$ and the robustness in the error estimator to effectively refine the inner layers. Figures 7 and 8 show the convergence plots for $r_\kappa = 10^4$ and $r_\kappa = 10^6$, respectively. We obtain optimal rates for different polynomial degrees in the \mathbb{V}_h and L_2 norms for all discrete approximations on the refined-mesh sequences.

5.6. 3D Eriksson-Johnson problem

We use a 3D version of the classical Eriksson-Johnson problem described in [45, 74]. We solve the equation (36) in the domain $\Omega = [0, 1]^3$ with diffusion coefficient $\kappa = 10^{-2}$, velocity field $\beta = (1, 0, 0)^T$ and a source term $f = 0$. We impose Dirichlet boundary conditions from the analytical solution:

$$u_{exa} = \frac{\exp(r_1(x-1)) - \exp(r_2(x-1))}{\exp(-r_1) - \exp(-r_2)} \sin(\pi y),$$

with $r_{1,2} = 1 \pm \sqrt{1 + 4\kappa^2\pi^2}/2\kappa$. Figure 9 shows the coarse and fine scales for the problem for linear polynomials, $p = 1$, and how the adaptive strategy captures the regions with sharp gradients, constructing

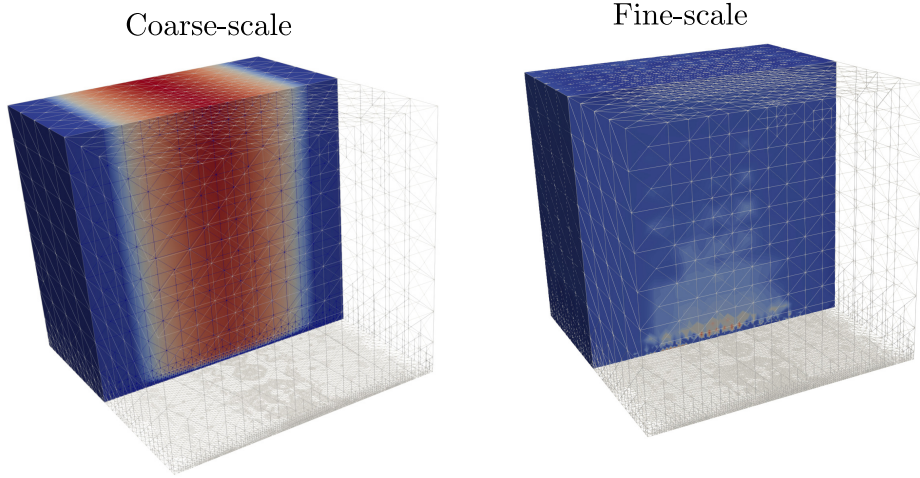


Figure 9: Coarse- & fine-scale approximations for the 3D Eriksson-Johnson problem

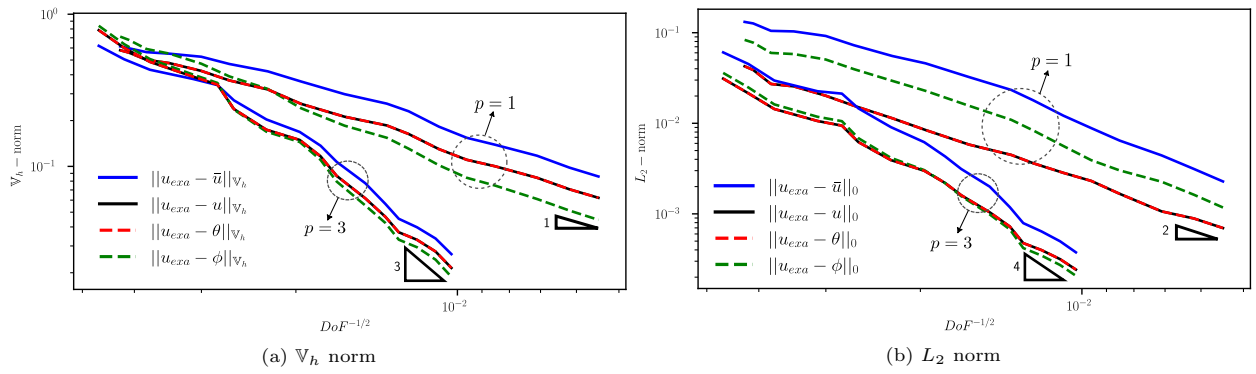


Figure 10: \mathbb{V}_h - and L_2 -norm convergence for 3D Eriksson-Johnson problem, $p = 1, 3$

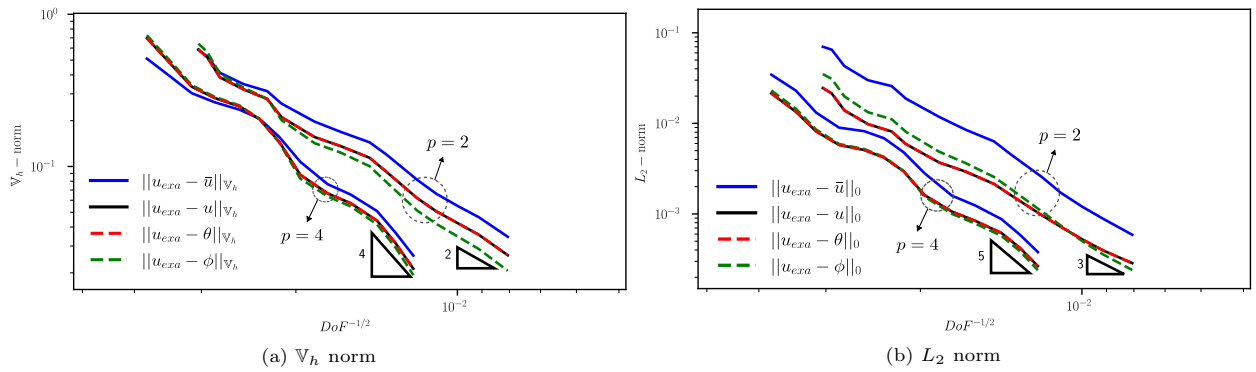


Figure 11: \mathbb{V}_h - and L_2 -norm convergence for 3D Eriksson-Johnson problem, $p = 2, 4$

a smooth solution. Figures 10 and 11 show the optimal convergence plot in \mathbb{V}_h and L_2 norms for the coarse- and full-scale approximations. As before, the adjoint multiscale reconstruction improves the \mathbb{V}_h norm and

the pre-asymptotic convergence, especially for lower-order polynomials.

6. Extension to nonlinear conservation laws

This section presents a numerical stability analysis for the nonlinear conservation law for our variational multiscale reconstructions. First, we formulate the discrete problem using the Lax-Friedrich flux for the nonlinear advective flux within the discontinuous Galerkin (dG) framework. Then, we describe the variational multiscale method for nonlinear problems [83] and specialize it to the adaptive stabilized finite element method [68] to obtain a nonlinear fine-scale approximation. We present some numerical results for Burgers' equation to demonstrate the accuracy and efficiency of our approach.

6.1. Discontinuous Galerkin discretization

We consider the following nonlinear conservation law:

$$\begin{aligned} \nabla \cdot (\mathbf{f}(u) - \kappa \nabla u) &= f, & \text{in } \Omega, \\ u &= u_D, & \text{on } \Gamma_D, \end{aligned} \quad (41)$$

where $\mathbf{f}(u)$ represents a nonlinear convective flux; thus, the dG discrete problem reads:

$$\begin{cases} \text{Find } u \in \mathbb{V}_h, \text{ such that:} \\ n_h(v; u) = \ell_h(v), \quad \forall v \in \mathbb{V}_h, \end{cases} \quad (42)$$

where $n(v; u)$ represents the nonlinear form including a SWIP contribution in (8) and the Lax-Friedrichs numerical flux Φ for the nonlinear convective flux defined as follows:

$$n_h(v; u) = b_h(v, u)^{\text{swip}} - \sum_{K \in \mathfrak{I}} (\nabla_h v, \mathbf{f}(u))_K + \sum_{F \in \mathcal{S}_h} ([v], \Phi)_F, \quad (43)$$

with,

$$\begin{aligned} \forall F \in \mathcal{S}_h^0, \quad \Phi &:= \frac{1}{2} (\mathbf{f}(u_1) \cdot \mathbf{n}_F + \mathbf{f}(u_2) \cdot \mathbf{n}_F + \eta_f (u_1 - u_2)), \\ \forall F \in \mathcal{S}_h^D, \quad \Phi &:= \frac{1}{2} (\mathbf{f}(u) \cdot \mathbf{n}_F + \eta_f u) + \frac{1}{2} (\mathbf{f}(u_D) \cdot \mathbf{n}_F - \eta_f u_D). \end{aligned} \quad (44)$$

η_f is a local dissipation parameter and is chosen based on the maximum eigenvalue of the flux function Jacobian. In equation (61), we set

$$\begin{aligned} \forall F \in \mathcal{S}_h^0, \quad \eta_f &:= \max_{w=u_1, u_2} |\mathbf{f}'(w) \cdot \mathbf{n}_F|, \\ \forall F \in \mathcal{S}_h^D, \quad \eta_f &:= |\mathbf{f}'(u) \cdot \mathbf{n}_F|. \end{aligned} \quad (45)$$

The right-hand side in (42) for weakly imposed non-homogeneous Dirichlet boundary conditions reads:

$$\begin{aligned} \ell_h(v) &:= \sum_{K \in \mathfrak{I}} (v, f) + \sum_{F \in \mathcal{S}_h^D} (n_e \kappa(v, u_D)_F - (\kappa \nabla_h v \cdot \mathbf{n}_F, u_D)_F) \\ &\quad - \sum_{F \in \mathcal{S}_h^D \cap \Gamma} \frac{1}{2} (v, \mathbf{f}(u_D) \cdot \mathbf{n}_F - \eta_f u_D)_F. \end{aligned} \quad (46)$$

We endow \mathbb{V}_h with the norm:

$$\|w\|_{\mathbb{V}_h}^2 := \|w\|_{\text{swip}}^2 + \|w\|_{\text{conv}}^2, \quad (47)$$

with $\|w\|_{\text{swip}}^2$ the SWIP norm contribution (14) and $\|w\|_{\text{conv}}^2$ a convective norm defined as follows:

$$\|w\|_{\text{conv}}^2 := \|w\|_0^2 + \sum_{F \in \mathcal{S}_h} \|[w]\|_{0,F}^2 + \sum_{K \in \mathfrak{I}} h_K \|\nabla w\|_{0,K}^2. \quad (48)$$

6.2. Residual minimization formulation

Following the residual minimization formulation in Section 3, and the nonlinear approach for residual minimization problems [73], we formulate the following nonlinear saddle-point problem to obtain the coarse-scale solution and an error estimate:

$$\begin{cases} \text{Find } (\varepsilon, \bar{u}) \in \mathbb{V}_h \times \bar{\mathbb{V}}_h, \text{ such that:} \\ g(v, \varepsilon) + n_h(v; \bar{u}) = l_h(v), & \forall v \in \mathbb{V}_h, \\ n'_h(\varepsilon, \bar{w}; \bar{u}) = 0, & \forall \bar{w} \in \bar{\mathbb{V}}_h. \end{cases} \quad (49)$$

Here, $n'_h(v, u; \delta u)$ is the linearized form of the nonlinear operator (43), evaluated at $\bar{u} \in \mathbb{V}_h$, and defined through the discrete Gâteaux derivative in the direction $\delta \bar{u} \in \bar{\mathbb{V}}_h$ as:

$$n'_h(v; \delta \bar{u}, \bar{u}) := \left. \frac{d}{d\varepsilon} n_h(v; \bar{u} + \varepsilon \delta \bar{u}) \right|_{\varepsilon=0}. \quad (50)$$

We use the Newton-Raphson method to solve (49) so that at each step of the nonlinear iteration, we solve the following linear problem:

$$\begin{cases} \text{Given } (\varepsilon_i, \bar{u}_i), \text{ find } (\delta \varepsilon, \delta \bar{u}) \in \mathbb{V}_h \times \bar{\mathbb{V}}_h, \text{ such that:} \\ g(v, \delta \varepsilon) + n'_h(v, \delta \bar{u}; \bar{u}_i) = l_h(v) - g(v, \varepsilon_i) - n_h(v, \bar{u}_i) & \forall v \in \mathbb{V}_h, \\ n'_h(\delta \varepsilon, \bar{w}; \bar{u}_i) = -n'_h(\varepsilon_i, \bar{w}; \bar{u}_i) & \forall \bar{w} \in \bar{\mathbb{V}}_h, \end{cases} \quad (51)$$

where we update u_i and ε_i at every iteration i such that:

$$\bar{u}_{i+1} = \bar{u}_i + k \delta \bar{u}, \quad \varepsilon_{i+1} = \varepsilon_i + k \delta \varepsilon \quad (52)$$

and assume convergence when $\|\bar{u}_{i+1} - \bar{u}_i\|_{\mathbb{V}_h} < 10^{-6}$. We use a damped Newton algorithm to solve the corresponding nonlinear saddle point problem. We denote the relaxation parameter as k in (52), following [91] (see algorithmic details in [73]). Regarding error estimation, we adopt a similar approach to that used in the linear problem. Here, ε in equation (49) represents the residual error of the nonlinear operator, i.e., $g(v, \varepsilon) = l_h(v) - n_h(v; \bar{u})$. However, we use the updated residual error (ε_{i+1}) to guide adaptivity after the solution of (51) converges.

6.3. Nonlinear variational multiscale method

Following the previous section, a natural approach to solve (42) uses the resulting linearized equation and updates the solution with a correction term at every iteration as:

$$u_{i+1} = u_i + \delta u. \quad (53)$$

In a multiscale context, both u_i and δu in (53) are decomposed into fine-scale ($\tilde{u}_i, \delta \tilde{u}$) and coarse-scale ($\bar{u}_i, \delta \bar{u}$) components. To circumvent the need for decomposing u_i at each iteration, we use a decoupled scale system by employing the subsequent approximation, as suggested by [83]:

$$u_i \approx \bar{u}_i,$$

which assumes the following at each iteration,

$$u_{i+1} \approx \bar{u}_{i+1} + \delta \tilde{u}. \quad (54)$$

We simplify the notation in (54) by dropping the sub-index i :

$$u \approx \bar{u} + \delta \tilde{u}. \quad (55)$$

From this, we define a multiscale formulation through defining a nonlinear direct sum decomposition for both the trial and test function spaces:

$$u = \bar{u} + \delta\tilde{u} \quad \forall u \in \mathbb{V}_h, \quad (56)$$

$$v = \hat{v} + v' \quad \forall v \in \mathbb{V}_h, \quad (57)$$

where $\bar{u} \in \bar{\mathbb{V}}_h$, $\delta\tilde{u} \in \tilde{\mathbb{V}}_h$, $\hat{v} \in \hat{\mathbb{V}}_h$, and $v' \in \mathbb{V}'_h$. Using (56) in the nonlinear problem (42), and a first-order Taylor expansion about the coarse-scale solution \bar{u} , the nonlinear form becomes:

$$n_h(v; u) = n_h(v; \bar{u} + \delta\tilde{u}) \approx n_h(v; \bar{u}) + n'_h(v; \delta\tilde{u}, \bar{u}) \quad v \in \mathbb{V}_h. \quad (58)$$

Drawing from the first equation in the nonlinear saddle-point problem in (49) and employing (42) and (58), we obtain the following identity:

$$\begin{cases} \text{Find } \delta\tilde{u} \in \mathbb{V}_h, \text{ such that:} \\ n'_h(v, \delta\tilde{u}; \bar{u}) = g(v, \varepsilon) \quad \forall v \in \mathbb{V}_h. \end{cases} \quad (59)$$

Here, we use ε and \bar{u} from (49) after the system converges. Similar to the linear case, in the subsequent sections, we represent the reconstructed full-scale solution (Equation (56)) as (u) and the dG solution in (42) as (θ) . Unlike the linear problem, u is not equivalent to θ , but rather an approximation of θ (i.e., $u \approx \theta$). The decoupled multiscale formulation substantially reduces computational costs by eliminating the need for explicit decomposition of u_i into coarse- and fine-scale components during each iteration. Instead, the decomposition is only performed once at each iteration level. In the next section, we demonstrate that our approach and the adaptive strategy yield an accurate and stable approximation of the coarse-scale solution and error indicator. This approximation enables the recovery of the full-scale solution following refinement.

6.4. Adjoint multiscale reconstruction

As for the linear case, we introduce an adjoint multiscale reconstruction ϕ defined as:

$$\phi = \bar{u} + \delta\check{u},$$

where $\delta\check{u}$ is fine-scale adjoint reconstruction, such that:

$$\begin{cases} \text{Find } \delta\check{u} \in \mathbb{V}_h, \text{ such that:} \\ n'_h(v, \delta\check{u}; \bar{u}) = g(v, \varepsilon') + n'_h(\varepsilon', v; \bar{u}) \quad \forall v \in \mathbb{V}_h. \end{cases} \quad (60)$$

The following example shows the improved accuracy of the adjoint reconstruction (ϕ) for the asymptotic regime in the energy norm (i.e., $\|u_{\text{exa}} - \phi\|_{\mathbb{V}_h} \lesssim \|u_{\text{exa}} - u\|_{\mathbb{V}_h}$).

6.5. Burgers' equation

This section assesses the performance of the proposed variational multiscale reconstructions applied to a nonlinear problem. We focus on the steady Burgers' equation, a widely used partial differential equation for modelling physical phenomena, including fluid dynamics, shock waves, and traffic flow. Subsequent sections will showcase results derived from this equation's isotropic and anisotropic variations.

6.5.1. Isotropic Burgers' equation

In the first example, we solve the isotropic case where $f(u) := \frac{\mathbf{b}u^2}{2}$ with $\mathbf{b} = [1, 1]^T$. The problem reads:

$$\begin{aligned} \nabla \cdot \left(\frac{\mathbf{b}u^2}{2} \right) - \kappa \Delta u &= f, & \text{in } \Omega, \\ u &= u_D, & \text{on } \Gamma_D, \end{aligned} \quad (61)$$

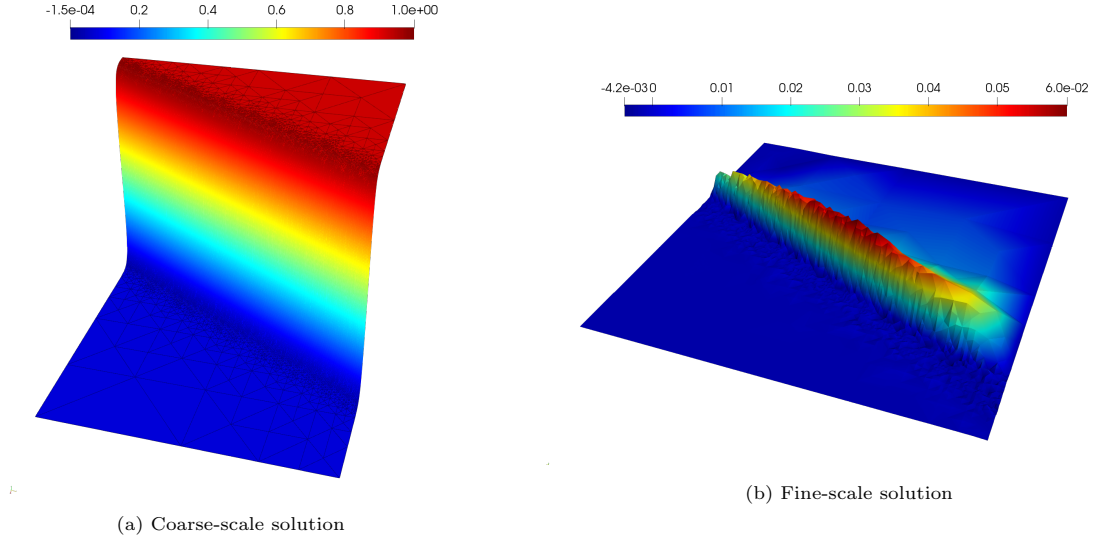


Figure 12: Solution for Burgers' equation for $\kappa = 10^{-3}$ & $p = 1$

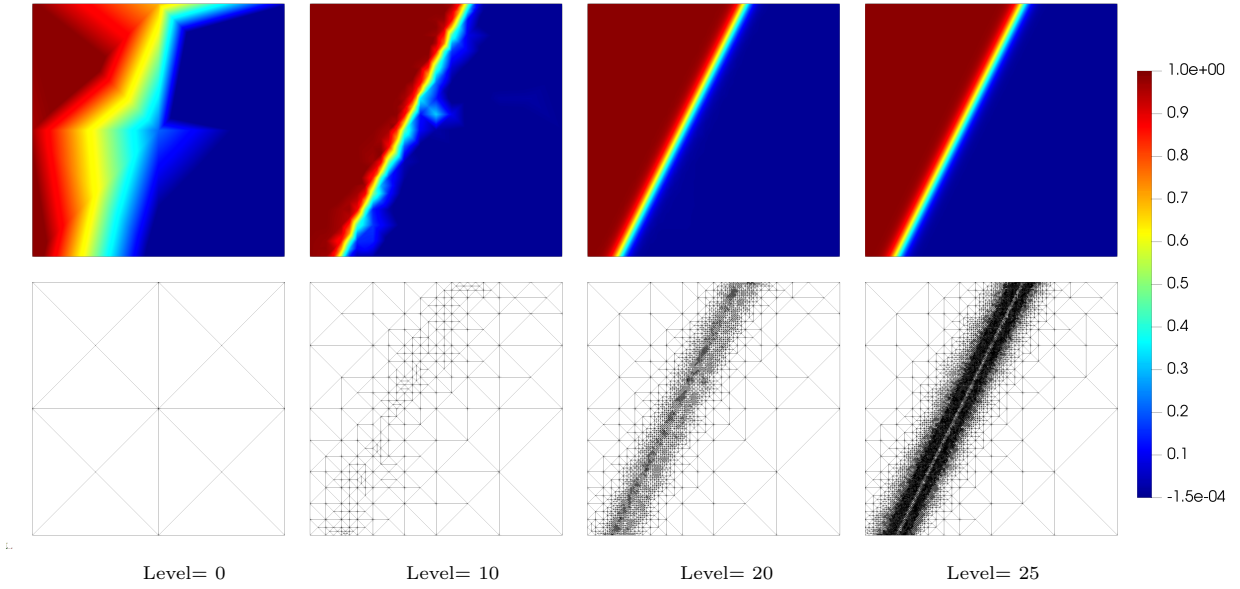


Figure 13: Solution for the isotropic Burgers equation for different refinement levels at $\kappa = 10^{-3}$

with $\Omega = [0, 1]^2$, $\kappa = 10^{-3}$ and a initial condition $u_0 = 0.5$ which rises to a inner discontinuity. We impose the source term f and Dirichlet boundary condition (u_D) from the exact solution:

$$u_{exa} = \frac{1}{2} \left(1 - \tanh \left(\frac{2x - y - 0.25}{\sqrt{5}\kappa} \right) \right).$$

We use $f'(w) = \mathbf{b}w$ to impose the local dissipation parameter in (45).

Figure 12 shows solution plots for $p = 1$, illustrating the smooth approach of the continuous solution and its correction for the fine-scale along the discontinuity. Figure 13 displays a sequence of four refinement levels to demonstrate the effectiveness of the refinement strategy in capturing the sharp inner layer, irrespective

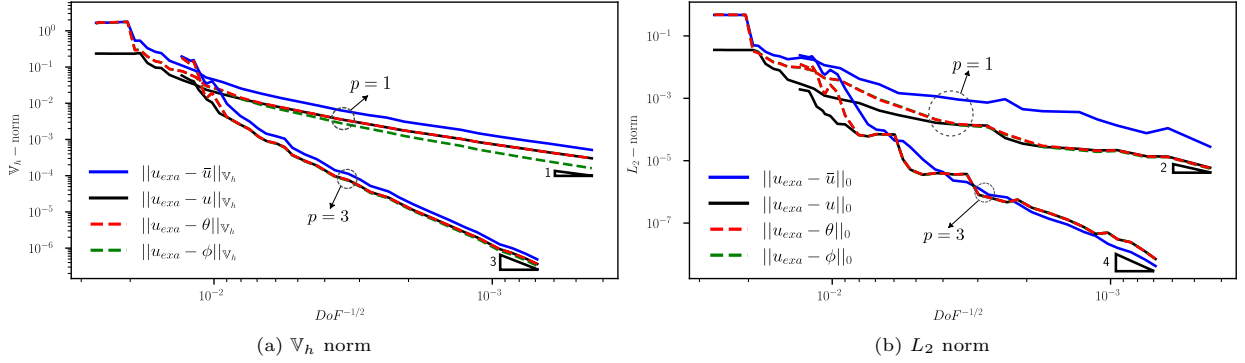


Figure 14: Convergence plots for Burgers' equation in the L_2 and \mathbb{V}_h norms, $p = 1, 3$

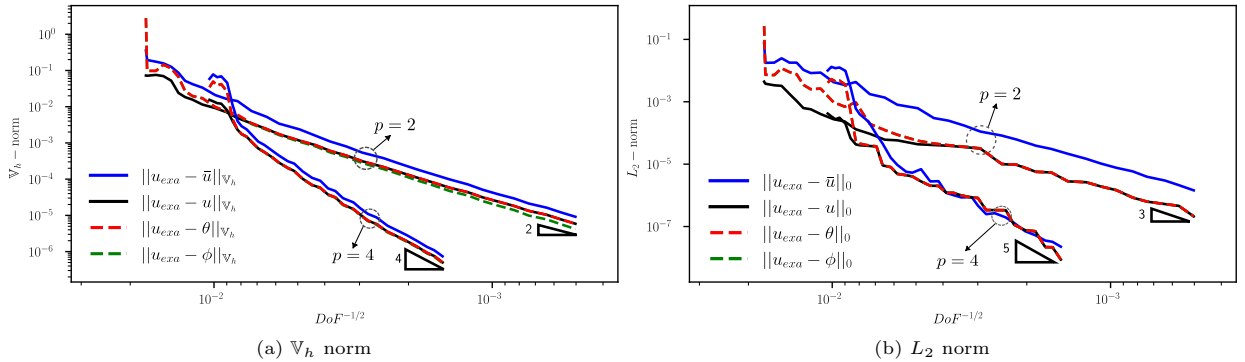


Figure 15: Convergence plots for Burgers' equation in the L_2 and \mathbb{V}_h norms, $p = 2, 4$

of the initial mesh. Figures 14 and 15 depict optimal convergence rates for $p = 1, 2, 3, 4$ in the L_2 and \mathbb{V}_h norms. Moreover, we show our method recovers the full-scale solution (i.e., $u \approx \theta$) after refinement, regardless of the polynomial order. Furthermore, as in the linear case, the adjoint multiscale reconstruction (ϕ) enhances the approximation quality in the \mathbb{V}_h norm.

6.5.2. Single-component Burgers' equation

We introduce a second scenario to test the numerical performance in the presence of a sharp shock layer. We select a problem from [92] to solve Burgers' equation in a single component, such that $f(u) := \left[\frac{u^2}{2}, u \right]^T$. This problem represents a challenge, especially for convection-dominated problems, due to the shock presence at $x = 0$. The problem reads:

$$\frac{1}{2} \frac{\partial u^2}{\partial x} + \frac{\partial u}{\partial y} = \kappa \left(\frac{\partial^2 u}{\partial x^2} + \frac{\partial^2 u}{\partial y^2} \right), \quad \text{in } \Omega, \quad (62)$$

with $\Omega = [0, 1]^2$ and initial guess $u_0 = 1 - 2x$. We impose Dirichlet boundary conditions $u_D = u_0$ at $y = 0$, $x = 0$ and $x = 1$ and zero Neumann boundary conditions at $y = 1$. The local dissipation parameter in (45) uses $f'(w) = [u, 1]$. We used a polynomial degree of $p = 3$ and a uniform element size of 4×4 for the initial mesh. Figure 16 illustrates the coarse and fine solutions for $\kappa = 10^{-2}$, $\kappa = 10^{-3}$, and $\kappa = 10^{-4}$. Additionally, Figure 17 demonstrates how the adaptive strategy effectively reduces oscillations along the shock for coarse meshes, regardless of the initial mesh [92].

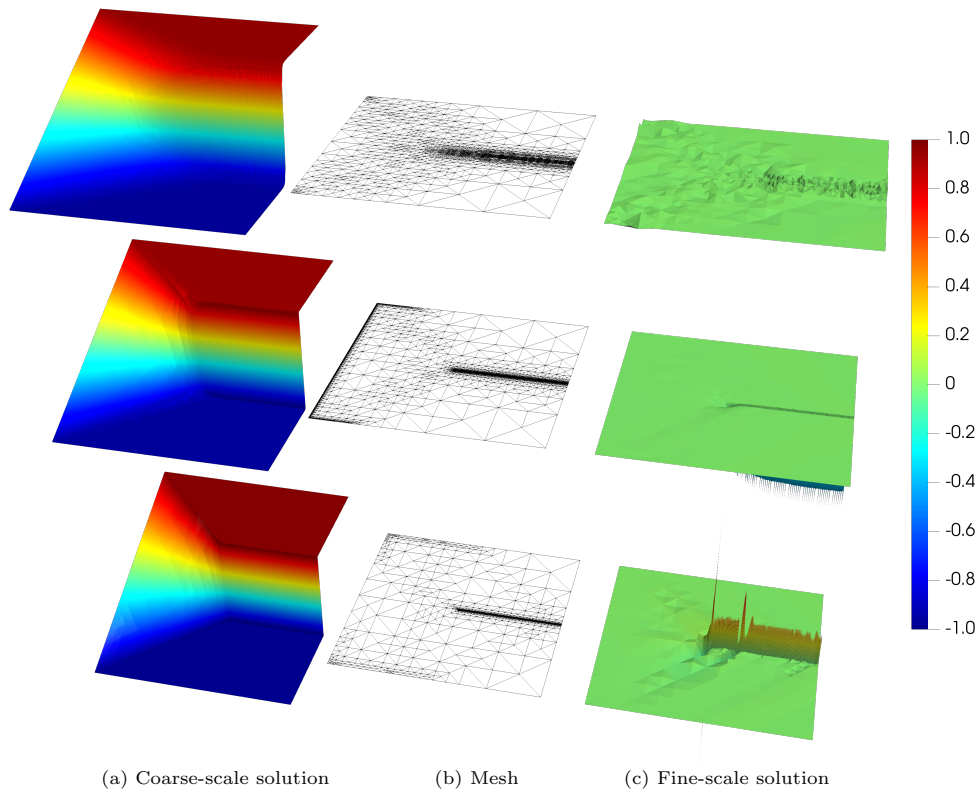


Figure 16: Coarse-scale solution and scale approximations for different diffusivities. (top: $\kappa = 10^{-2}$, middle: $\kappa = 10^{-3}$, bottom: $\kappa = 10^{-4}$)

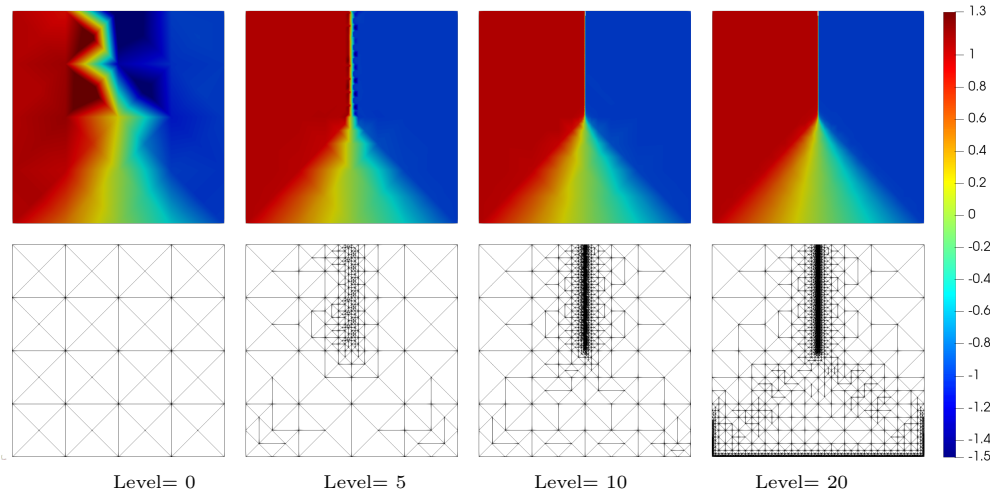


Figure 17: Solution for the Burgers equation for different refinement levels at $\kappa = 10^{-2}$

7. Conclusions

We introduce an adaptive stabilized finite element method for convective-dominated diffusion problems using variational multiscale fine-scale reconstructions. The method constructs a coarse-scale approximation

by minimizing the residual in dual discontinuous Galerkin norm and employs a robust error estimation technique to obtain a fine-scale solution and guide adaptivity. We show the effectiveness and reliability of our method through various numerical experiments involving different types of linear problems, such as highly heterogeneous, strong anisotropic diffusion tensors, and convection-dominated diffusion. Lastly, we successfully extend the method to solve the nonlinear conservation law. We use Burgers' equation as an example where we obtain stable solutions and optimal convergence rates.

8. Acknowledgments

This work is supported by the close collaboration between Curtin University and CSIRO. under the CSIRO DEI FSP postgraduate top-up scholarship (Grant no. 50068868). J.G. gratefully acknowledges Roberto Rocca Education Program for its support.

References

- [1] A. N. Brooks, T. J. Hughes, Streamline upwind/petrov-galerkin formulations for convection dominated flows with particular emphasis on the incompressible navier-stokes equations, *Computer methods in applied mechanics and engineering* 32 (1982) 199–259.
- [2] T. J. R. Hughes, L. P. Franca, G. M. Hulbert, A new finite element formulation for computational fluid dynamics: VIII. The Galerkin/Least-Squares method for advection-diffusive equations, *Comput. Methods Appl. Mech. Engrg.* 73 (1989) 173–89.
- [3] V. John, P. Knobloch, S. B. Savescu, A posteriori optimization of parameters in stabilized methods for convection–diffusion problems – part i, *Computer Methods in Applied Mechanics and Engineering* 200 (2011) 2916–29.
- [4] T. J. Hughes, G. R. Feijóo, L. Mazzei, J. B. Quincy, The variational multiscale method—a paradigm for computational mechanics, *Computer Methods in Applied Mechanics and Engineering* 166 (1998) 3–24.
- [5] T. J. Hughes, L. Mazzei, K. E. Jansen, Large eddy simulation and the variational multiscale method, *Computing and visualization in science* 3 (2000) 47–59.
- [6] Y. Bazilevs, V. Calo, J. Cottrell, T. Hughes, A. Reali, G. Scovazzi, Variational multiscale residual-based turbulence modeling for large eddy simulation of incompressible flows, *Computer Methods in Applied Mechanics and Engineering* 197 (2007) 173–201.
- [7] Y. Bazilevs, C. Michler, V. Calo, T. Hughes, Isogeometric variational multiscale modeling of wall-bounded turbulent flows with weakly enforced boundary conditions on unstretched meshes, *Computer Methods in Applied Mechanics and Engineering* 199 (2010) 780–90. *Turbulence Modeling for Large Eddy Simulations*.
- [8] K. Chang, T. Hughes, V. Calo, Isogeometric variational multiscale large-eddy simulation of fully-developed turbulent flow over a wavy wall, *Computers & Fluids* 68 (2012) 94–104.
- [9] Y. Ghaffari Motlagh, H. T. Ahn, T. J. Hughes, V. M. Calo, Simulation of laminar and turbulent concentric pipe flows with the isogeometric variational multiscale method, *Computers & Fluids* 71 (2013) 146–55.
- [10] K. Garikipati, T. Hughes, A variational multiscale approach to strain localization–formulation for multidimensional problems, *Computer Methods in Applied Mechanics and Engineering* 188 (2000) 39–60.
- [11] A. Masud, R. Calderer, A variational multiscale stabilized formulation for the incompressible navier–stokes equations, *Computational Mechanics* 44 (2009) 145–60.
- [12] A. Masud, K. Xia, A variational multiscale method for inelasticity: Application to superelasticity in shape memory alloys, *Computer methods in applied mechanics and engineering* 195 (2006) 4512–31.
- [13] J. Baiges, R. Codina, Variational multiscale error estimators for solid mechanics adaptive simulations: An orthogonal subgrid scale approach, *Computer Methods in Applied Mechanics and Engineering* 325 (2017) 37–55.
- [14] R. Codina, On stabilized finite element methods for linear systems of convection-diffusion-reaction equations, *Computer Methods in Applied Mechanics and Engineering* 188 (2000) 61–82.
- [15] S. Badia, R. Codina, Unified stabilized finite element formulations for the stokes and the darcy problems, *SIAM J. Numer. Anal.* 47 (2009) 1971–2000.
- [16] R. Codina, S. Badia, J. Baiges, J. Principe, Variational multiscale methods in computational fluid dynamics, *Encyclopedia of computational mechanics* (2018) 1–28.
- [17] T. J. R. Hughes, G. Sangalli, Variational multiscale analysis: the fine-scale green's function, projection, optimization, localization, and stabilized methods, *SIAM J. Numer. Anal.* 45 (2007) 539–57.
- [18] R. Codina, Stabilization of incompressibility and convection through orthogonal sub-scales in finite element methods, *Computer Methods in Applied Mechanics and Engineering* 190 (2000) 1579–99.
- [19] R. Codina, Analysis of a stabilized finite element approximation of the oseen equations using orthogonal subscales, *Applied Numerical Mathematics* 58 (2008) 264–83.
- [20] R. Codina, Stabilized finite element approximation of transient incompressible flows using orthogonal subscales, *Computer Methods in Applied Mechanics and Engineering* 191 (2002) 4295–321.
- [21] T. J. Hughes, Multiscale phenomena: Green's functions, the Dirichlet-to-Neumann formulation, subgrid scale models, bubbles and the origins of stabilized methods, *Computer methods in applied mechanics and engineering* 127 (1995) 387–401.

- [22] A. Masud, R. Khurram, A multiscale/stabilized finite element method for the advection–diffusion equation, *Computer Methods in Applied Mechanics and Engineering* 193 (2004) 1997–2018.
- [23] G. Hauke, G. Sangalli, M. H. Doweidar, Combining adjoint stabilized methods for the advection-diffusion-reaction problem, *Mathematical Models and Methods in Applied Sciences* 17 (2007) 305–26.
- [24] S. Tran, O. Sahni, Finite element-based large eddy simulation using a combination of the variational multiscale method and the dynamic smagorinsky model, *Journal of Turbulence* 18 (2017) 391–417.
- [25] A. A. Oberai, P. M. Pinsky, A multiscale finite element method for the helmholtz equation, *Computer Methods in Applied Mechanics and Engineering* 154 (1998) 281–97.
- [26] D. Sondak, J. Shadid, A. Oberai, R. Pawlowski, E. Cyr, T. Smith, A new class of finite element variational multiscale turbulence models for incompressible magnetohydrodynamics, *Journal of Computational Physics* 295 (2015) 596–616.
- [27] O. Colomés, S. Badia, R. Codina, J. Principe, Assessment of variational multiscale models for the large eddy simulation of turbulent incompressible flows, *Computer Methods in Applied Mechanics and Engineering* 285 (2015) 32–63.
- [28] I. Akkerman, S. J. Hulshoff, K. G. van der Zee, R. de Borst, *Variational Germano Approach for Multiscale Formulations*, Springer Netherlands, Dordrecht, 2011, pp. 53–73.
- [29] Z. Wang, A. Oberai, Spectral analysis of the dissipation of the residual-based variational multiscale method, *Computer Methods in Applied Mechanics and Engineering* 199 (2010) 810–8. *Turbulence Modeling for Large Eddy Simulations*.
- [30] A. Cohen, W. Dahmen, G. Welper, Adaptivity and variational stabilization for convection-diffusion equations, *ESAIM: Mathematical Modelling and Numerical Analysis* 46 (2012) 1247–73.
- [31] L. Demkowicz, J. Gopalakrishnan, A class of discontinuous Petrov–Galerkin methods. Part I: The transport equation, *Computer Methods in Applied Mechanics and Engineering* 199 (2010) 1558–72.
- [32] L. Demkowicz, J. Gopalakrishnan, A class of discontinuous Petrov–Galerkin methods. II. optimal test functions, *Numerical Methods for Partial Differential Equations* 27 (2011) 70–105.
- [33] L. Demkowicz, J. Gopalakrishnan, Analysis of the DPG method for the Poisson equation, *SIAM Journal on Numerical Analysis* 49 (2011) 1788–809.
- [34] L. F. Demkowicz, N. Heuer, Robust DPG method for convection-dominated diffusion problems, *SIAM J. Numer. Anal.* 51 (2013) 2514–37.
- [35] L. F. Demkowicz, J. Gopalakrishnan, A primal DPG method without a first-order reformulation, *Comput. Math. Appl.* 66 (2013) 1058–64.
- [36] C. Carstensen, L. F. Demkowicz, J. Gopalakrishnan, A posteriori error control for DPG methods, *SIAM J. Numer. Anal.* 52 (2014) 1335–53.
- [37] C. Carstensen, L. F. Demkowicz, J. Gopalakrishnan, Breaking spaces and forms for the DPG method and applications including Maxwell equations, *Comput. Math. Appl.* 72 (2015) 494–522.
- [38] J. Zitelli, I. Muga, L. Demkowicz, J. Gopalakrishnan, D. Pardo, V. Calo, A class of discontinuous Petrov–Galerkin methods. Part IV: The optimal test norm and time-harmonic wave propagation in 1D, *Journal of Computational Physics* 230 (2011) 2406–32.
- [39] A. H. Niemi, N. O. Collier, V. M. Calo, Automatically stable discontinuous Petrov–Galerkin methods for stationary transport problems: Quasi-optimal test space norm, *Computers & Mathematics with Applications* 66 (2013) 2096–113. *ICNC-FSKD 2012*.
- [40] D. Broersen, W. Dahmen, R. P. Stevenson, On the stability of DPG formulations of transport equations, *Math. Comput.* 87 (2015) 1051–82.
- [41] A. H. Niemi, N. O. Collier, V. M. Calo, Discontinuous Petrov–Galerkin method based on the optimal test space norm for one-dimensional transport problems, *Procedia Computer Science* 4 (2011) 1862–9. *Proceedings of the International Conference on Computational Science, ICCS 2011*.
- [42] A. H. Niemi, N. O. Collier, V. M. Calo, Discontinuous Petrov–Galerkin method based on the optimal test space norm for steady transport problems in one space dimension, *Journal of Computational Science* 4 (2013) 157–63. *Agent-Based Simulations, Adaptive Algorithms, ICCS 2011 Workshop*.
- [43] W. Dahmen, C. Huang, C. Schwab, G. Welper, Adaptive petrov-galerkin methods for first order transport equations, *SIAM J. Numer. Anal.* 50 (2011) 2420–45.
- [44] V. M. Calo, N. O. Collier, A. H. Niemi, Analysis of the discontinuous Petrov–Galerkin method with optimal test functions for the Reissner–Mindlin plate bending model, *Computers & Mathematics with Applications* 66 (2014) 2570–86.
- [45] J. Chan, J. A. Evans, A minimum-residual finite element method for the convection-diffusion equation, *Technical Report*, Texas Univ at Austin inst for computational engineering and science, 2013.
- [46] P. Binev, W. Dahmen, R. A. DeVore, Adaptive finite element methods with convergence rates, *Numerische Mathematik* 97 (2004) 219–68.
- [47] W. H. Reed, T. R. Hill, *Triangular mesh methods for the neutron transport equation*, Technical Report, Los Alamos Scientific Lab., N. Mex.(USA), 1973.
- [48] D. N. Arnold, F. Brezzi, B. Cockburn, L. Donatella Marini, Unified analysis of discontinuous Galerkin methods for elliptic problems, *SIAM Journal on Numerical Analysis* 39 (2001) 1749–79.
- [49] B. Ayuso, L. D. Marini, Discontinuous Galerkin methods for advection-diffusion-reaction problems, *SIAM J. Numer. Anal.* 47 (2009) 1391–420.
- [50] B. Cockburn, G. E. Karniadakis, C.-W. Shu, *Discontinuous Galerkin methods: theory, computation and applications*, volume 11, Springer Science & Business Media, 2012.
- [51] D. A. Di Pietro, A. Ern, *Mathematical aspects of discontinuous Galerkin methods*, volume 69, Springer Science & Business Media, 2011.
- [52] A. Ern, J.-L. Guermond, *Theory and practice of finite elements*, Springer, ????

- [53] C. Johnson, J. Pitkäranta, An analysis of the discontinuous Galerkin method for a scalar hyperbolic equation, *Mathematics of computation* 46 (1986) 1–26.
- [54] F. Brezzi, B. Cockburn, L. D. Marini, E. Süli, Stabilization mechanisms in discontinuous Galerkin finite element methods, *Computer Methods in Applied Mechanics and Engineering* 195 (2006) 3293–310.
- [55] P. Bochev, T. J. Hughes, G. Scovazzi, A multiscale discontinuous Galerkin method, in: *International Conference on Large-Scale Scientific Computing*, Springer, 2005, pp. 84–93.
- [56] A. Buffa, T. J. Hughes, G. Sangalli, Analysis of a multiscale discontinuous Galerkin method for convection-diffusion problems, *SIAM Journal on Numerical Analysis* 44 (2006) 1420–40.
- [57] T. J. Hughes, G. Scovazzi, P. B. Bochev, A. Buffa, A multiscale discontinuous Galerkin method with the computational structure of a continuous Galerkin method, *Computer Methods in Applied Mechanics and Engineering* 195 (2006) 2761–87.
- [58] G. Sangalli, A discontinuous residual-free bubble method for advection-diffusion problems, *Journal of engineering mathematics* 49 (2004) 149–62.
- [59] C. Coley, J. A. Evans, Variational multiscale modeling with discontinuous subscales: analysis and application to scalar transport, *Meccanica* 53 (2018) 1241–69.
- [60] S. K. Stoter, B. Cockburn, T. J. Hughes, D. Schillinger, Discontinuous Galerkin methods through the lens of variational multiscale analysis, *Computer Methods in Applied Mechanics and Engineering* 388 (2022) 114220.
- [61] I. Babuška, M. Zlámal, Nonconforming elements in the finite element method with penalty, *SIAM J. Numer. Anal.* 10 (1973) 863–75.
- [62] J. Douglas, Jr., T. Dupont, Interior penalty procedures for elliptic and parabolic Galerkin methods, in: *Computing methods in applied sciences (Second Internat. Sympos., Versailles, 1975)*, Lecture Notes in Phys., Vol. 58, Springer, Berlin, 1976, pp. 207–16.
- [63] E. Burman, P. Hansbo, Edge stabilization for Galerkin approximations of convection-diffusion-reaction problems, *Comput. Methods Appl. Mech. Engrg.* 193 (2004) 1437–53.
- [64] E. Burman, P. Zunino, A domain decomposition method based on weighted interior penalties for advection-diffusion-reaction problems, *SIAM Journal on Numerical Analysis* 44 (2006) 1612–38.
- [65] E. Burman, A. Ern, Continuous interior penalty *hp*-finite element methods for advection and advection-diffusion equations, *Math. Comp.* 76 (2007) 1119–40.
- [66] E. Burman, A. Ern, Stabilized Galerkin approximation of convection-diffusion-reaction equations: discrete maximum principle and convergence, *Math. Comp.* 74 (2005) 1637–52.
- [67] E. Burman, A posteriori error estimation for interior penalty finite element approximations of the advection-reaction equation, *SIAM J. Numer. Anal.* 47 (2009) 3584–607.
- [68] V. M. Calo, A. Ern, I. Muga, S. Rojas, An adaptive stabilized conforming finite element method via residual minimization on dual discontinuous Galerkin norms, *Computer Methods in Applied Mechanics and Engineering* (2020).
- [69] L. F. Demkowicz, W. Rachowicz, P. R. B. Devloo, A fully automatic *hp*-adaptivity, *Journal of Scientific Computing* 17 (2002) 117–42.
- [70] L. Vardapetyan, L. F. Demkowicz, *hp*-adaptive finite elements in electromagnetics, *Computer Methods in Applied Mechanics and Engineering* 169 (1999) 331–44.
- [71] M. Paszyński, L. F. Demkowicz, Parallel, fully automatic *hp*-adaptive 3d finite element package, *Engineering with Computers* 22 (2006) 255–76.
- [72] P. Binev, W. Dahmen, R. A. DeVore, P. Petrushev, Approximation classes for adaptive methods, *Serdica. Mathematical Journal* 28 (2002) 391–416.
- [73] R. J. Cier, S. Rojas, V. M. Calo, A nonlinear weak constraint enforcement method for advection-dominated diffusion problems, *Mechanics Research Communications* 112 (2021) 103602.
- [74] R. J. Cier, S. Rojas, V. M. Calo, Automatically adaptive, stabilized finite element method via residual minimization for heterogeneous, anisotropic advection–diffusion–reaction problems, *Computer Methods in Applied Mechanics and Engineering* 385 (2021) 114027.
- [75] V. Calo, M. Łoś, Q. Deng, I. Muga, M. Paszyński, Isogeometric residual minimization method (igrm) with direction splitting preconditioner for stationary advection-dominated diffusion problems, *Computer Methods in Applied Mechanics and Engineering* 373 (2021) 113214.
- [76] S. Rojas, D. Pardo, P. Behnoudfar, V. M. Calo, Goal-oriented adaptivity for a conforming residual minimization method in a dual discontinuous Galerkin norm, *Computer Methods in Applied Mechanics and Engineering* 377 (2021) 113686.
- [77] M. Łoś, S. Rojas, M. Paszyński, I. Muga, V. M. Calo, DGIRM: Discontinuous Galerkin based isogeometric residual minimization for the Stokes problem, *Journal of Computational Science* 50 (2021) 101306.
- [78] F. E. Kyburg, S. Rojas, V. M. Calo, Incompressible flow modeling using an adaptive stabilized finite element method based on residual minimization, *International Journal for Numerical Methods in Engineering* 123 (2022) 1717–35.
- [79] T. Poulet, J. F. Giraldo, E. Ramanaidou, A. Piechocka, V. M. Calo, Paleo-stratigraphic permeability anisotropy controls supergene mimetic martite goethite deposits, *Basin Research* (2022).
- [80] J. F. Giraldo, V. M. Calo, An adaptive in space, stabilized finite element method via residual minimization for linear and nonlinear unsteady advection–diffusion–reaction equations, *Mathematical and Computational Applications* 28 (2023) 7.
- [81] N. A. Labanda, L. Espath, V. M. Calo, A spatio-temporal adaptive phase-field fracture method, *Computer Methods in Applied Mechanics and Engineering* 392 (2022) 114675.
- [82] J. G. Hasbani, P. Sepúlveda, I. Muga, V. M. Calo, S. Rojas, Adaptive stabilized finite elements via residual minimization onto bubble enrichments, 2023. [arXiv:2303.17982](https://arxiv.org/abs/2303.17982).
- [83] R. Juanes, T. W. Patzek, Multiscale-stabilized solutions to one-dimensional systems of conservation laws, *Computer methods in Applied Mechanics and Engineering* 194 (2005) 2781–805.

- [84] J. Vovelle, Convergence of finite volume monotone schemes for scalar conservation laws on bounded domains, *Numerische Mathematik* 90 (2002) 563–96.
- [85] A. Ern, A. F. Stephansen, P. Zunino, A discontinuous Galerkin method with weighted averages for advection–diffusion equations with locally small and anisotropic diffusivity, *IMA Journal of Numerical Analysis* 29 (2009) 235–56.
- [86] K. Shahbazi, An explicit expression for the penalty parameter of the interior penalty method, *Journal of Computational Physics* 205 (2005) 401–7.
- [87] R. E. Bank, B. D. Welfert, H. Yserentant, A class of iterative methods for solving saddle point problems, *Numerische Mathematik* 56 (1989) 645–66.
- [88] M. Alnæs, J. Blechta, J. Hake, A. Johansson, B. Kehlet, A. Logg, C. Richardson, J. Ring, M. E. Rognes, G. N. Wells, The FEniCS project version 1.5, *Archive of Numerical Software* 3 (2015).
- [89] W. F. Mitchell, A collection of 2d elliptic problems for testing adaptive grid refinement algorithms, *Applied mathematics and computation* 220 (2013) 350–64.
- [90] A. Pestiaux, S. Melchior, J.-F. Remacle, T. Kärrnä, T. Fichefet, J. Lambrechts, Discontinuous Galerkin finite element discretization of a strongly anisotropic diffusion operator, *International Journal for Numerical Methods in Fluids* 75 (2014) 365–84.
- [91] R. E. Bank, D. J. Rose, Global approximate Newton methods, *Numerische Mathematik* 37 (1981) 279–95.
- [92] D. Moro, N. Nguyen, J. Peraire, A hybridized discontinuous Petrov–Galerkin scheme for scalar conservation laws, *International journal for numerical methods in engineering* 91 (2012) 950–70.